Science Advances
AAAS

advances.sciencemag.org/cgi/content/full/6/32/eabb1342/DC1

Supplementary Materials for

Biomolecule-guided cation regulation for dendrite-free metal anodes

Jian Zhi, Shengkai Li, Mei Han, P. Chen*

*Corresponding author. Email: p4chen@uwaterloo.ca

Published 7 August 2020, *Sci. Adv.* **6**, eabb1342 (2020)
DOI: 10.1126/sciadv.abb1342

This PDF file includes:

DFT calculations
Calculating the mass of dissolved CH in the organic electrolyte during electrochemical cycling
Calculating the mass of dissolved CH in the aqueous electrolyte during electrochemical cycling
Puncture resistance measurement
Assembling of 200-Ah class battery
Notes S1 and S2
Figs. S1 to S25
Tables S1 to S5

DFT calculations

All DFT calculations were performed using the Vienna Ab-initio Simulation Package. The projector augmented-wave method combined with a plane wave basis set at a cutoff energy of 500 eV was used to describe the core and valence electrons. The Perdew–Burke–Ernzerhof functional was used in all the calculations. The ground-state atomic geometries of the carbon surfaces with and without Zn deposition were obtained by reducing the forces on each atom to below 0.02 eV Å−1. A Monkhorst-Pack k-point mesh scheme of 4 × 4 × 1 was used. The Zn metal surface was represented by a pristine double-layer C (6 × 6) super cell.

The Zn atom deposition was studied over the Zn metal surface at the nucleation site. Similarly, the interaction of a single Zn atom was calculated according to equation 1:

$$E_{ad(Zn)} = E_{surface+Zn} - (E_{surface} + E_{Zn}) \quad (1)$$

Calculating the mass of dissolved CH in organic electrolyte during electrochemical cycling

CH@AGM (disc, 0.95 cm^2) was prepared by immersing AGM in 5% aqueous CH solution, and the mass of absorbed CH in AGM was firstly obtained by weighing the mass of CH@AGM and subtracting the mass of AGM before CH coating. This CH@AGM was then sandwiched by two pieces of pristine AGM with the same area, and coupled with LMO and Li anode. After 10 cycles under 1C, the assembling kit was opened, and the sandwiched CH@AGM was taken out. As CH cannot be dissolved in EC and acetone under room temperature, $LiPF_6$ salts can be completely removed after rinsing with large quantity of EC, and the residue DMC:EC:DEC was then removed by rinsing with acetone. The mass of CH@AGM after cycling was weighed after drying in the

oven for 10 minutes. Finally, the mass of dissolved CH (M_{dis}) in organic electrolyte can be calculated by the following equation:

$$M_{dis} = M_{CH@AGM,after} - M_{CH@AGM,before} \quad (1)$$

Where $M_{CH@AGM,after}$ and $M_{CH@AGM,before}$ is the mass of CH@AGM before and after cycling, respectively.

And the content of dissolved CH in electrolyte can be calculated by:

$$C_{dis} = \frac{M_{dis}}{M_{ele}+M_{dis}} \times 100\% \quad (2)$$

where C_{dis} is the content of CH dissolved in electrolyte, M_{dis} and M_{ele} is the mass of dissolved CH and electrolyte, respectively.

The mass of dissolved CH after 50, 80 and 100 cycles were also calculated through the same method.

Calculating the mass of dissolved CH in aqueous electrolyte during electrochemical cycling

CH@AGM (square, 4 cm^2) was prepared by immersing AGM in 5% aqueous CH solution, and the mass of absorbed CH in AGM was firstly obtained by weighing the mass of CH@AGM and subtracting the mass of AGM before CH coating. This CH@AGM was then sandwiched by two pieces of pristine AGM with the same area, and coupled with LMO and Zn anode. After 10 cycles under 1C, the assembling kit was opened, and the sandwiched CH@AGM was taken out. As CH cannot be dissolved in water under room temperature, inorganic salts can be completely removed after rinsing with large quantity of water. The mass of CH@AGM after cycling was weighed after drying in the oven for 10 minutes. The mass of dissolved CH in aqueous electrolyte (M_{dis}), and the content of CH in aqueous electrolyte (C_{dis}) can be calculated through the same equation as shown above.

Puncture resistance measurement

The puncture resistance of CH@AGM was measured on a universal testing machine (Gotech Al3000) that was equipped with a 100 N load cell at a cross-head speed of 500 mm/min. Puncture

tests were performed according to ASTM F1342. A puncture needle probe A (round tip: R 0.010 ± 0.001″, length 2.00 ± 0.062″, diameter 0.080 ± 0.002″) was attached to the tensile joint and the locknut was screwed. The needle was moved downward onto the test specimen to allow the crosshead to build up the desired velocity prior to impacting the test specimen.

Assembling of 200-Ah class battery

(1) Cathode preparation

LMO, conductive carbon (KS-6), and carboxymethyl cellulose/Styrene-Butadiene Rubber (CMC/SBR) with a weight ratio of 85:10:5) were firstly mixed with N-Methyl-2-Pyrrolidinone (NMP). After mixing for 4 hours, the slurry was dip-coated on nylon mesh. After drying, the composite film was attached on both sides of graphite foil using CMC/SBR+KS-6 as binder. Then one graphite tab was attached on top of the graphite foil. The size of the fabriccated cathode was 210*150*1 mm.

(2) Anode preparation

Zinc powders, CMC and SBR with a weight ratio of 95:2.5:2.5 were mixed with NMP for 4 hours. Then the mixture was dip-coated on Cu foil. After drying, one Cu tab was attached on the bottom of the foil.

(3) battery assembling

One piece of cathode, two pieces of AGM (or one piece of AGM and one piece of CH@AGM), and one piece of anode were stacked together to obtain a single battery unit. Then 48 units were stacked togenther and assembled in a plastic battery pack. After adding electrolyte (1M $ZnSO_4$ and 2M Li_2SO_4), seven such battery packs were stacked together in a large battery pack to obtain a 200 Ah full battery. The tabs on the top of cathodes were converged to a large graphite tab connected to a Cu wire, while the tabs on the bottom of anodes were converged to a large Cu tab connected to a Cu wire.

The preparation method of 5 and 65 Ah-class batteries is the same as above, just with fewer single battery units and battery packs.

Supplementary note 1: characterizations of molecular-level binding of CH and Zn^{2+} by Raman spectra

Raman spectra of the samples were recorded using a 632.8-nm laser Raman spectrometer (Jobin Yvon Raman microspectrometer, HR 800). The samples were sealed in a capillary tube. The normalized spectra were deconvoluted using a Gaussian–Lorentzian function spectroscopic analysis. The binding number of CH towards Zn^{2+} can be evaluated from the intensity ratio of the bands from free and bonded CH through Irish's method. The Raman intensity of the bands at 1650 cm^{-1} (I_{free}) and 1680 cm^{-1} (I_{bind}) is determined by the concentration of free CH molecules ($[CH]_{free}$) and CH molecules bonded with Zn^{2+} ($[CH]_{bind}$). J_{bind} and J_{free} are the molar scattering coefficients for the bonded and free CH, respectively.

$$I_{free} = J_{free}\,[CH]_{free} \quad (3)$$

$$I_{bind} = J_{bind}\,[CH]_{bind} \quad (4)$$

$$[CH] = [CH]_{free} + [CH]_{bind} \quad (5)$$

$$\frac{[CH]_{free}}{[CH]_{bind}} = \frac{I_{free}}{I_{bind}}\frac{J_{bind}}{J_{free}} \quad (6)$$

So,

$$\frac{I_{bind}}{[CH]} = -\frac{J_{bind}}{J_{free}}\frac{I_{free}}{[CH]} + J_{bind} \quad (7)$$

Therefore, the J_{bind}/J_{free} value can be evaluated from the slope of the $I_{bind}/[CH]$ versus $I_{free}/[CH]$ plot. The solvation number of TEP molecules toward Li ions is derived from the following equation:

$$n_{CH} = \frac{[CH]_{bind}}{[Li^+]} = \frac{[CH]}{[Li^+](1 + \frac{[CH]_{free}}{[CH]_{bind}})} = \frac{[CH]}{[Li^+](1 + \frac{J_{bind}}{J_{free}}\frac{I_{free}}{I_{bind}})} \quad (8)$$

Supplementary note 2: characterization of molecular-level binding between CH and Li^+ by PFG-NMR

Diffusion coefficients of Li^+ and CH were measured using ^7Li and ^{15}N NMR in aqueous solution respectively, using a 300 MHz Bruker DPX300 and partly with 600 MHz Bruker 600 Avance III spectrometers. Before NMR test, the CH-Li^+ solution (LiOH in this study) was heated to 45 °C to ensure complete dissolution of CH. The pulsed field-gradient spin-echo (PFG-SE) NMR method was used to quantitatively investigate the binding of CH with Li^+ in the solution. Diffusion coefficients were extracted from the nonlinear least squares of the integrated resonance intensity as a function of the gradient amplitude. The resonance intensity of these integrals, I, and the diffusion coefficient, D, were related according to the following equation:

$$I = I_0 \exp\left[-D\left(\Delta - \frac{\delta}{3} - \frac{\tau}{2}\right)g^2\gamma^2\delta^2\right] \quad (9)$$

where I is the resonance intensity measure with pulse sequences, I_0 is the intensity of the resonance in the absence of a gradient pulse, D is the diffusion coefficient, Δ is the diffusion delay time, which defined the diffusional time scale, and γ is the gyromagnetic ratio. The parameters δ and g were the gradient pulse duration and amplitude, respectively. And τ is the delay between the positive and negative gradient pulses. The values of δ and Δ were fixed at 2 and 80ms for ^7Li and 2 and 50ms for ^{15}N, respectively. The gradient strength was varied in 16 equal steps with an appropriate maximum gradient strength to achieve a full decay of the echo profiles.

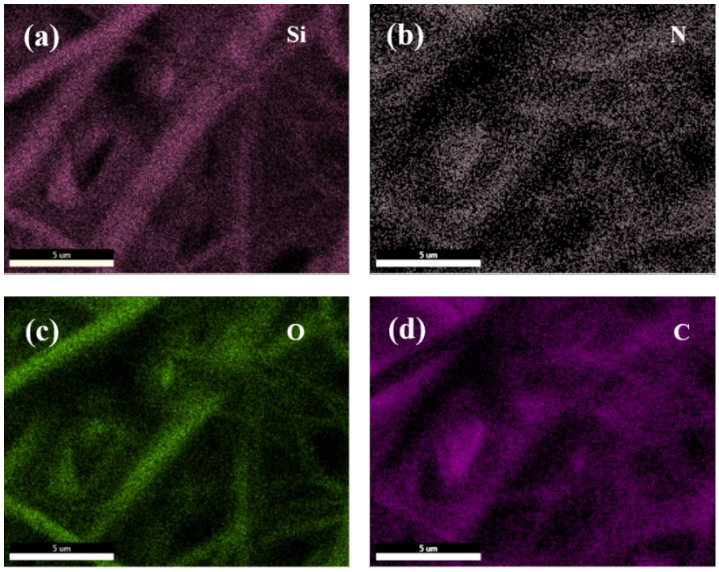

Figure S1. EDX maps of (a) Si, (b) N, (c) O and (d) C of CH@AGM.

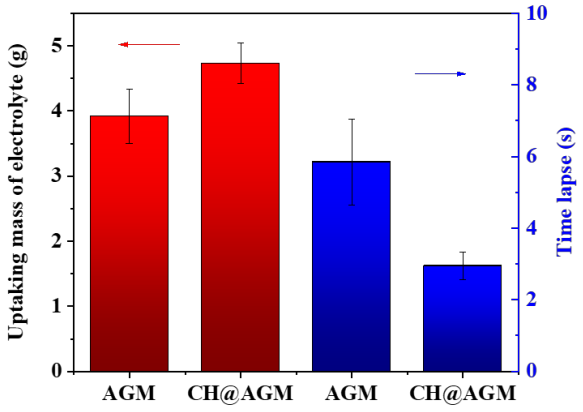

Figure S2. Uptaking mass of 1M $ZnSO_4$ and 2M Li_2SO_4 electrolyte in AGM separator and CH@AGM under vertical testing setup (red) and time lapse of AGM separator and CH@AGM in fully soaking 30μm 1M $ZnSO_4$ and 2M Li_2SO_4 electrolyte under horizontal testing setup (blue).

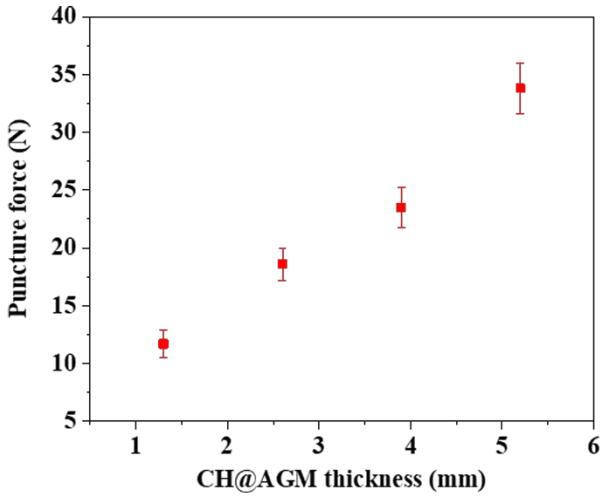

Figure S3. Puncture force of CH@AGM with different thickness.

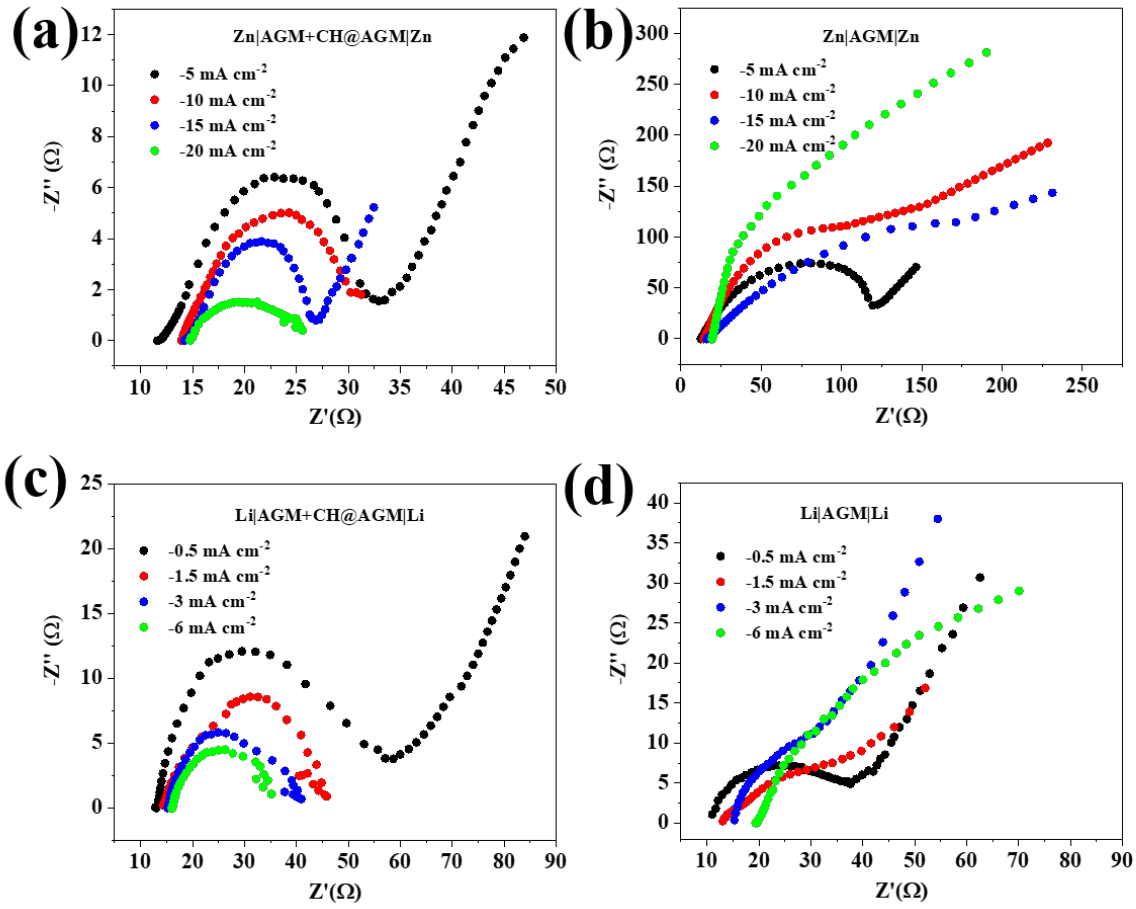

Figure S4. **Galvanostatic electrochemical impedance spectroscopies in symmetric Zn and Li cells at different direct current biases.** a,b) Nyquist plots of Zn|AGM+CH@AGM|Zn and Zn|AGM|Zn cells at -5,-10,-15 and -20 mA cm^{-2} direct current densities in 1M $ZnSO_4$ electrolyte. c,d) Nyquist plots of Li|AGM+CH@AGM|Li and Li|AGM|Li cells at -0.5, -1.5, -3 and -6 mA cm^{-2} direct current densities in 1M $LiPF_6$ in 1:1:1 DMC:EC:DEC electrolyte.

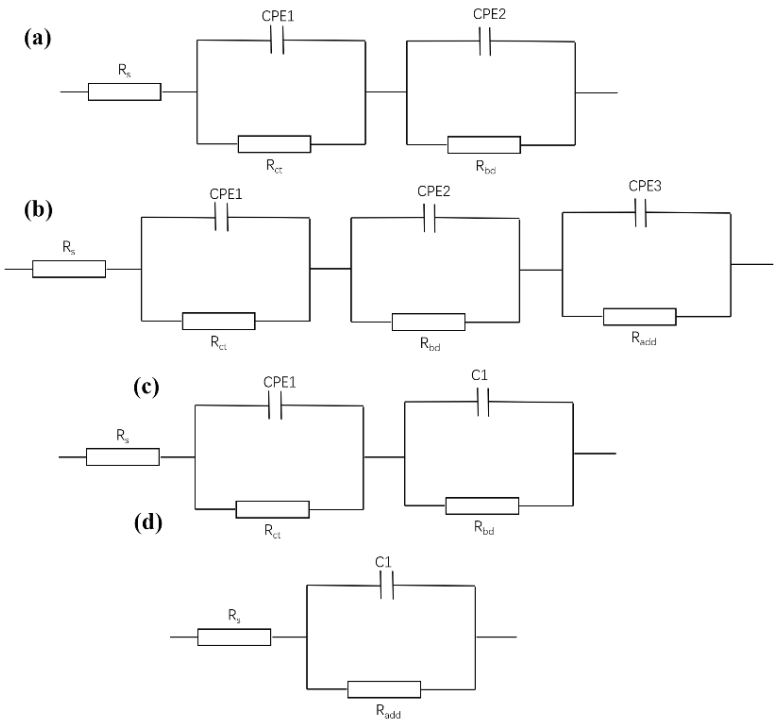

Figure S5. Equivalent circuit models for impedance data of (a) -10 and -20 mA cm^{-2} in **Figure (S4a)**, -1.5, -3 and -6 mA cm^{-2} in **Figure (S4c)**; (b) -5 and -15 mA cm^{-2} in **Figure (S4a)**,-5 mA cm^{-2} in **Figure S4b**, -0.5 mA cm^{-2} in **Figure (S4c)**, and -0.5 mA cm^{-2} in **Figure (S4d)**; (c) -1.5 mA cm^{-2} in **Figure (S4d)**; (d) -10, -15 and -20 mA cm^{-2} in **Figure (S4b)**, -3 and -6 mA cm^{-2} in **Figure (S4d)**. R_{add} corresponds to additional resistance to achieve a best fit.

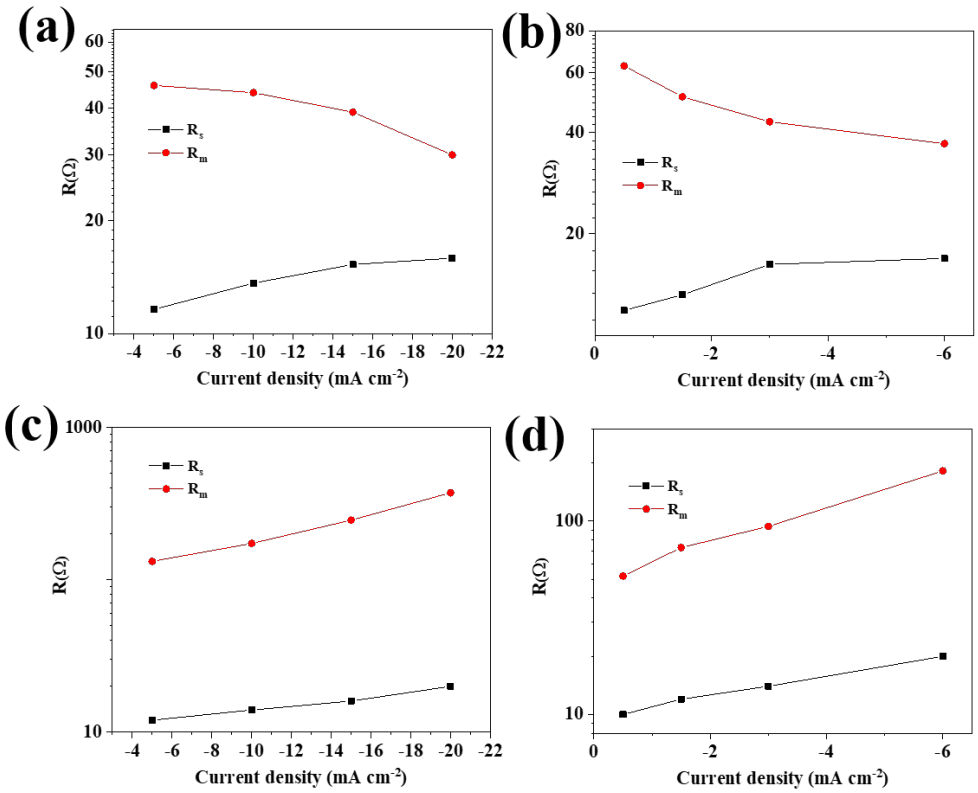

Figure S6. R_s and R_m as a function of different applied dc-biases in (a,b) Zn|AGM+CH@AGM|Zn and Li|AGM+CH@AGM|Li cells and (c,d) Zn|AGM|Zn and Li|AGM|Li cells.

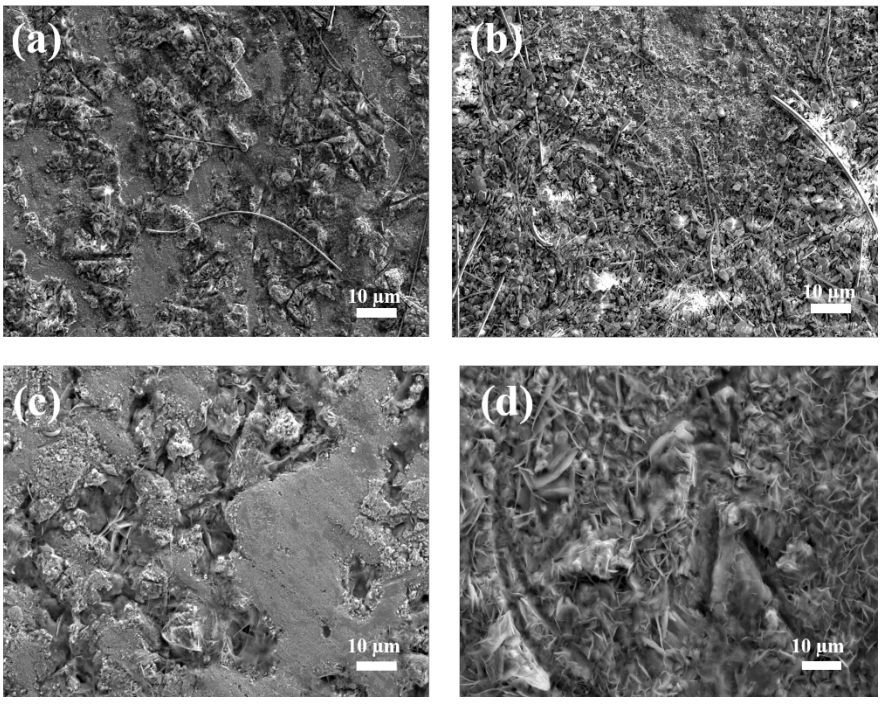

Figure S7. SEM images of Zn and Li electrode after 72-hours galvanostatic deposition at a current density of -1.5 mA cm^{-2} with (a,c) and without CH (b,d) in the separator.

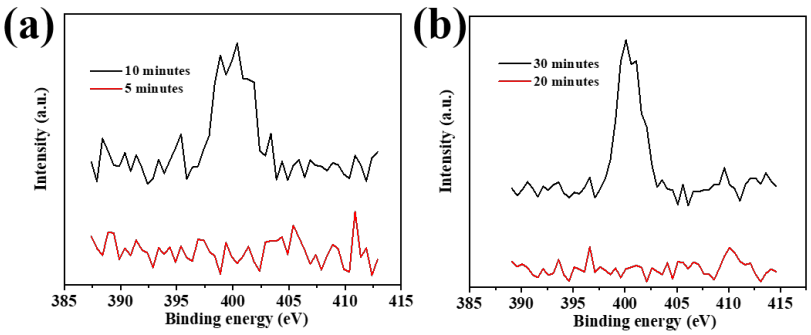

Figure S8. High-resolution XPS (N 1s) of (a) Zn anode and (b) Li anode after different time chronoamperometry

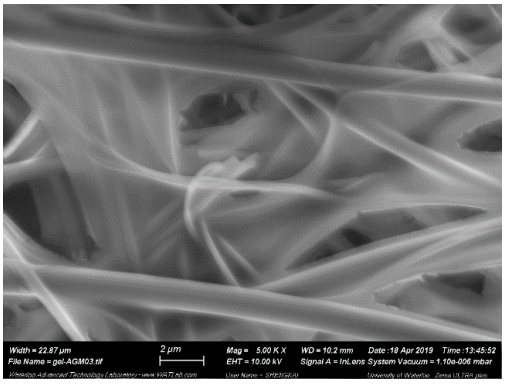

Figure S9. SEM of CH@AGM after 1-hour chronoamperometry.

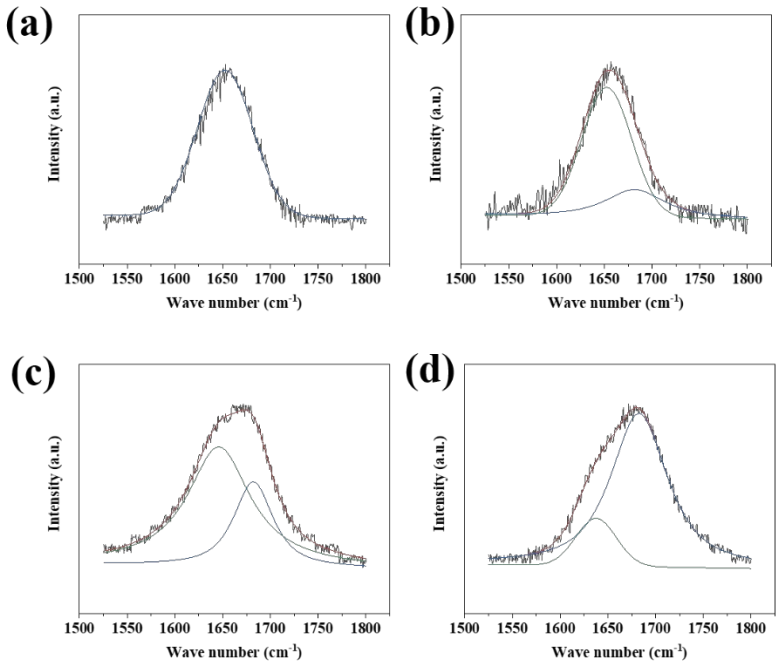

Figure S10. Raman spectra of 10^{-2} M CH aqueous solution (a) and $ZnSO_4$-CH electrolyte with $ZnSO_4$-CH mass ratios of 1:5 (b), 1:3 (c) and 1:1 (d) in 1500-1800 cm^{-1} range. Black dots and red solid lines represent the original spectra and the fitting results, respectively. The bands at 1590-1670 cm^{-1} is attributed to CH molecules. The peak at 1630-1740 cm^{-1} is attributed to the binding of CH with the Zn^{2+} ions. Curve fitting was performed with a Gaussian–Lorentz function.

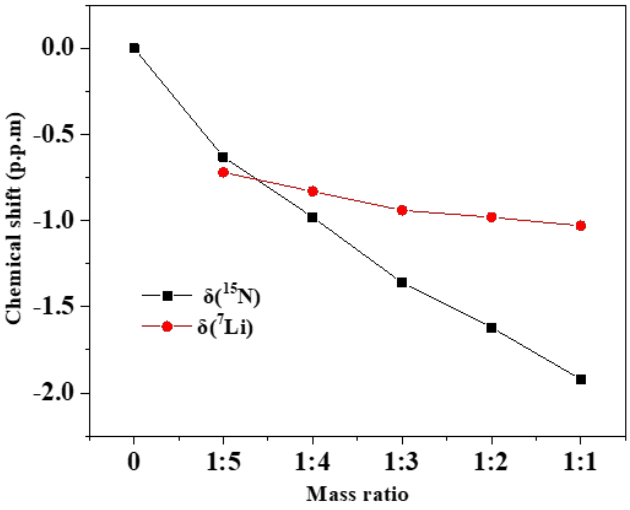

Figure S11. Change in chemical shift for ^{7}Li ($\delta(^{7}Li)$) and ^{15}N ($\delta(^{15}N)$) with different Li_2SO_4- CH mass ratios at 25 °C.

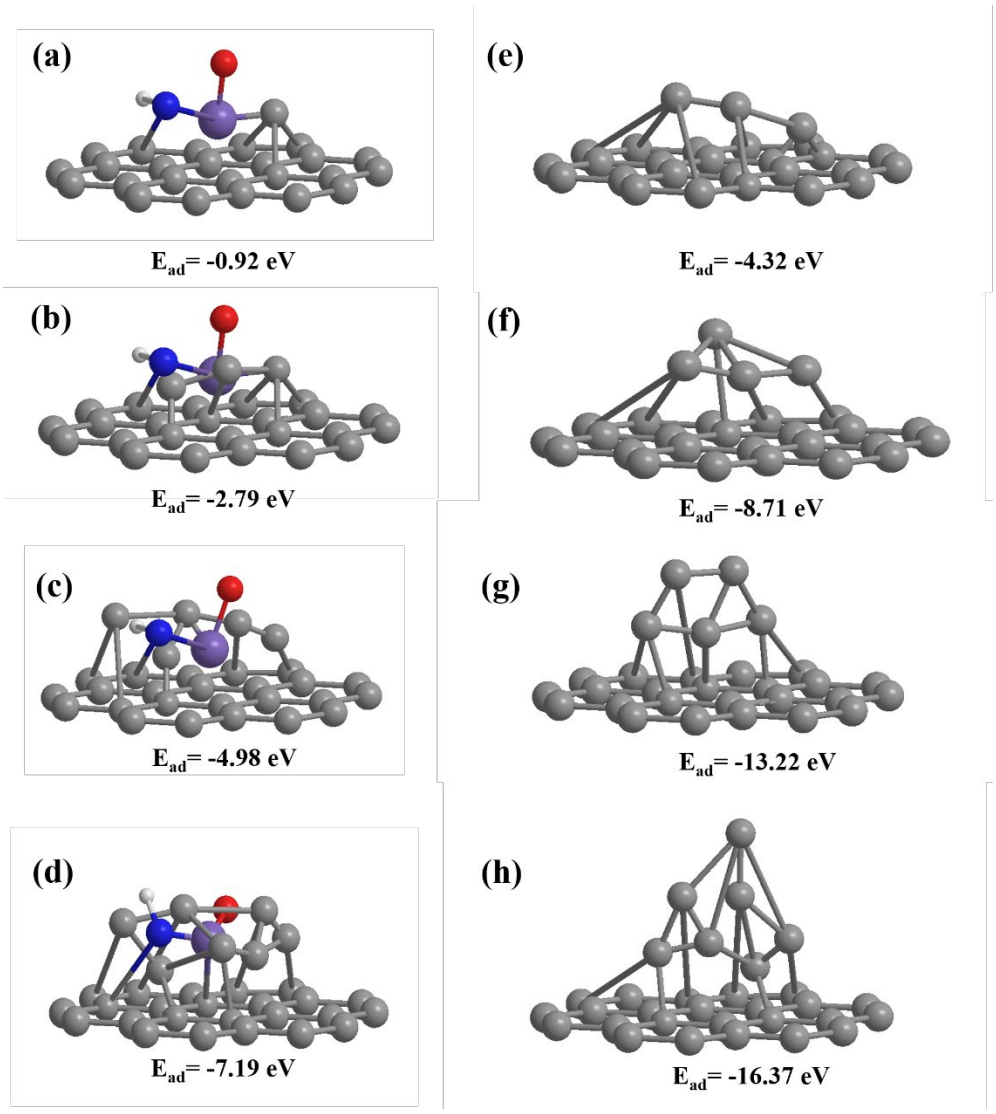

Figure S12. Simulation calculation of Zn nucleation on CH coils deposited Zn metal and pristine Zn metal. Left (a-d): Zn atom adsorption and segregation on Zn metal surface deposited with CH fine particles, in which an -NH-C=O functional group has been added on the surface. From (a) to (d) the Zn atom number is 1, 3, 5, and 7, respectively. Right (e-h): Zn atom adsorption and segregation on the pristine Zn metal surface. From (e) to (h) the Zn atom number is 1, 4, 5, and 7, respectively. The Zn, N, H, and O atoms are represented by gray, blue, white, and red balls, respectively.

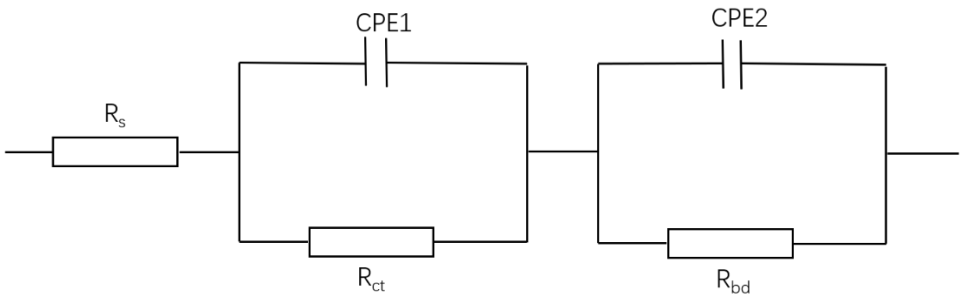

Figure S13. Relevant equivalent circuit model for impedance data in Figure 4g-j.

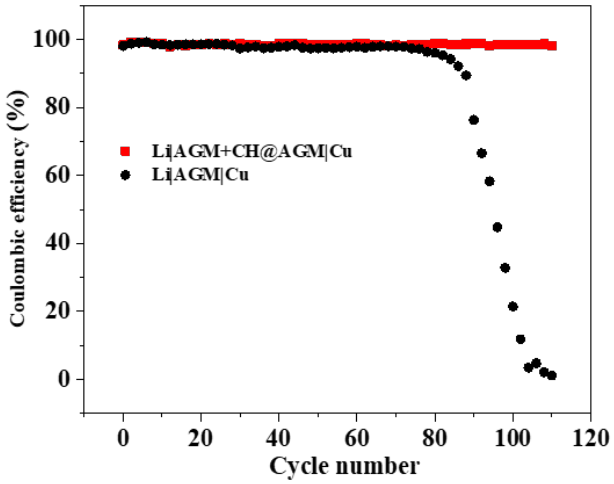

Figure S14. Coulombic efficiency (CE) of Li|AGM+CH@AGM|Cu and Li|AGM|Cu at a current density of 1 mA cm^{-2}.

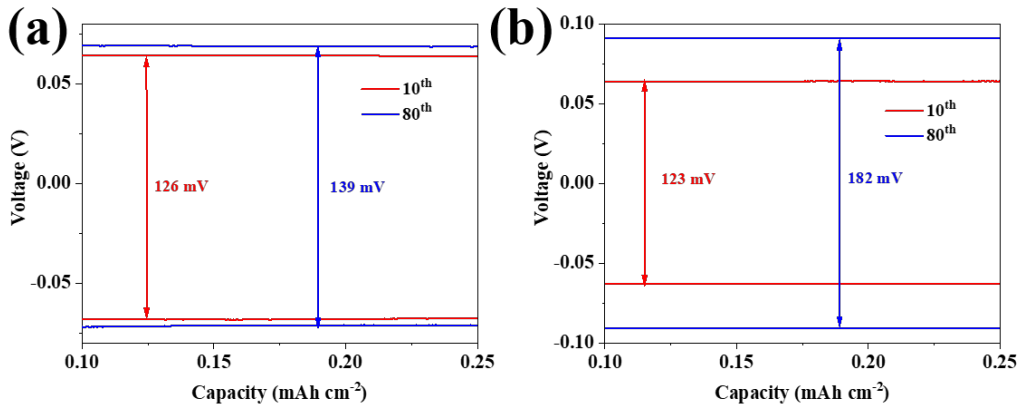

Figure S15. Polarization curves of plating/stripping process in (a) Li|AGM+CH@AGM|Cu and (b) Li|AGM|Cu after 10^{th} and 80^{th} cycle.

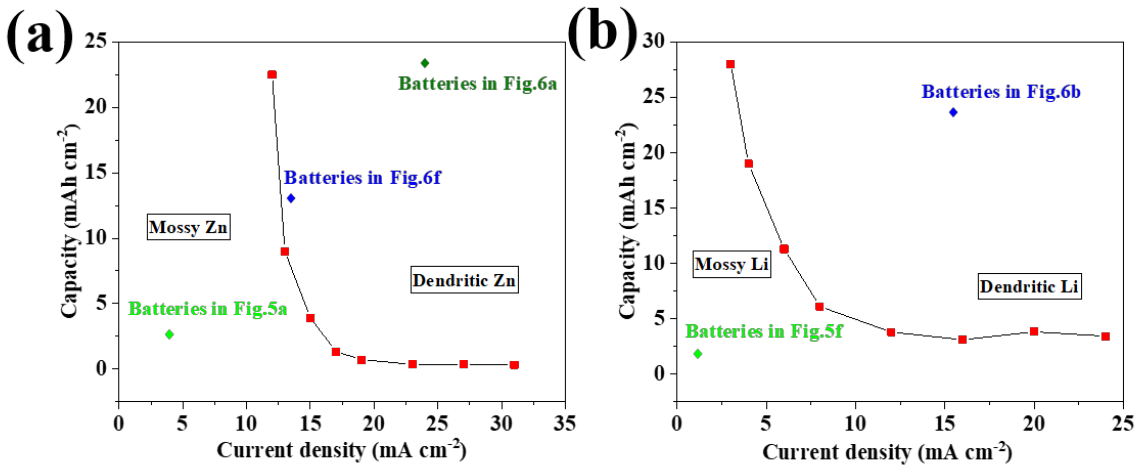

Figure S16. Current-dependent Sand's capacity in Zn (a) and Li (b) metal electrodes.

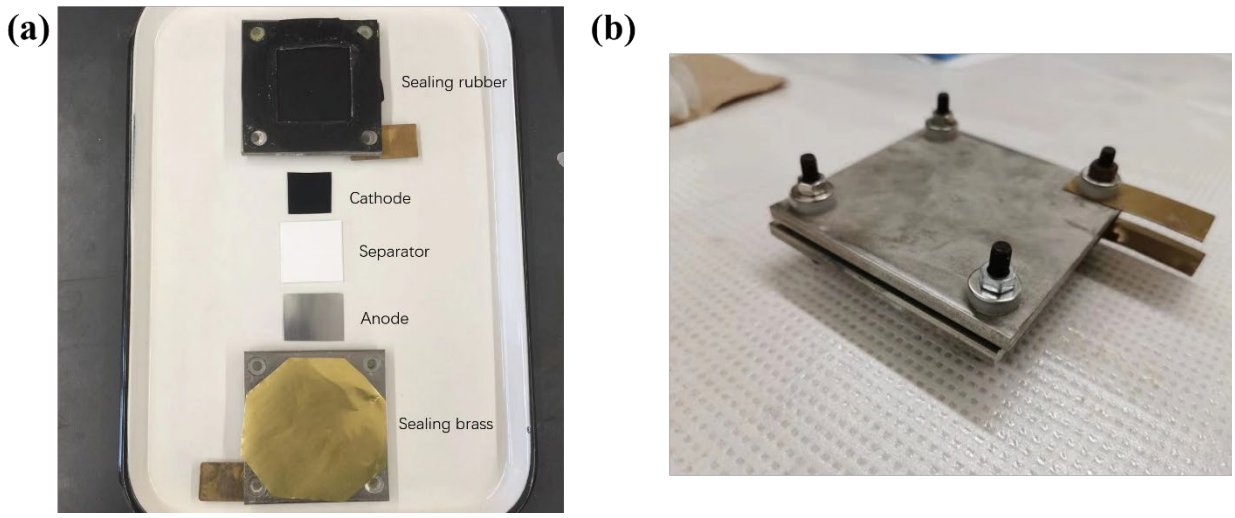

Figure S17. Battery configurations for Zn metal battery under unconstrained and constrained conditions, and Li metal battery under constrained conditions. (a) The components in the battery. (b) The assembled kit. The cathode, separator and anode vary in different batteries as shown in Table S1. Photo credit: Mei Han, University of Waterloo.

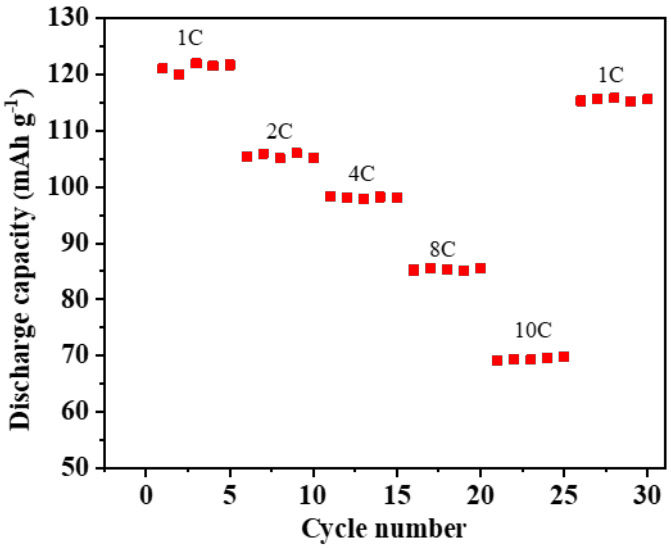

Figure S18. Charge-discharge capacities of LMO|g-AGM|Zn cell as a function of cycle number at different C rates. When the rate increased to 10 C, a discharge capacity of 69 mAh g^{-1} was still maintained. A capacity of 115.12 mAh g^{-1} was recoverable and sustainable up to 30 cycles without obvious loss when the current density returns to 1 C.

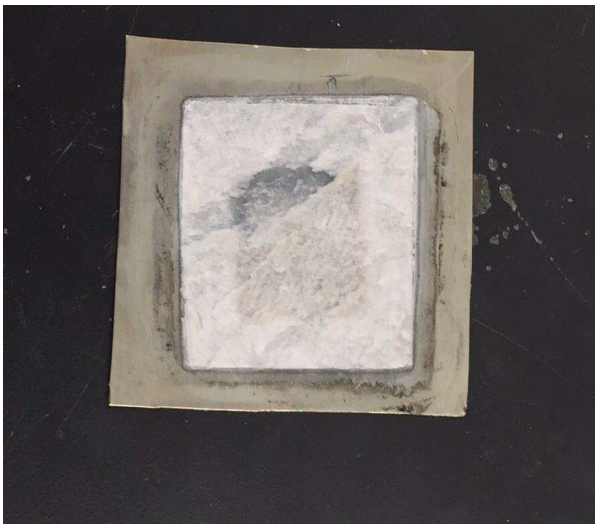

Figure S19. Image of separator in LMO|AGM+CH@AGM|Zn cell after 400 cycles under 60°C. Photo credit: Shengkai Li, University of Waterloo.

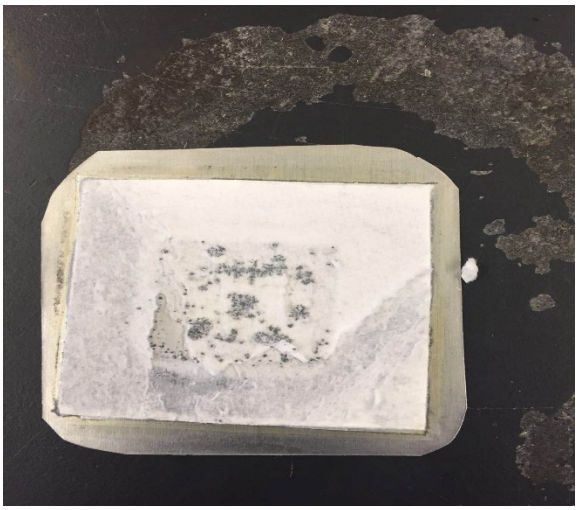

Figure S20. Image of separator in LMO|AGM|Zn cell after 400 cycles under 60℃. Photo credit: Shengkai Li, University of Waterloo.

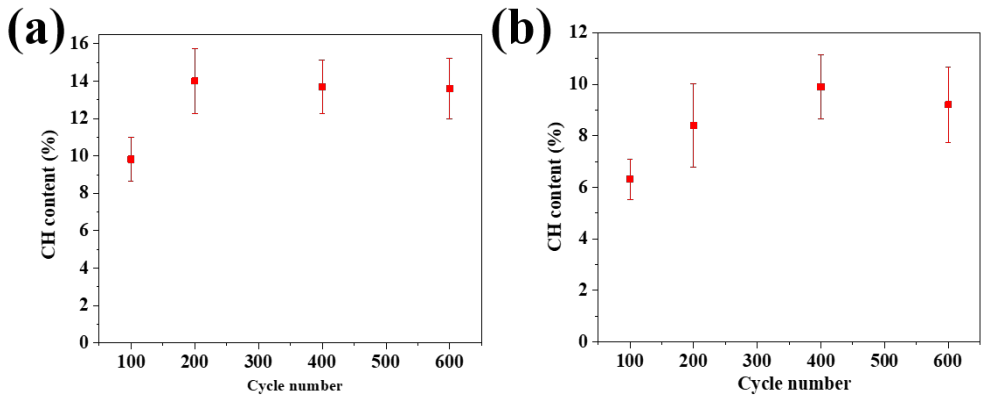

Figure S21. CH content in aqueous (a) and organic (b) electrolyte after different number of cycles.

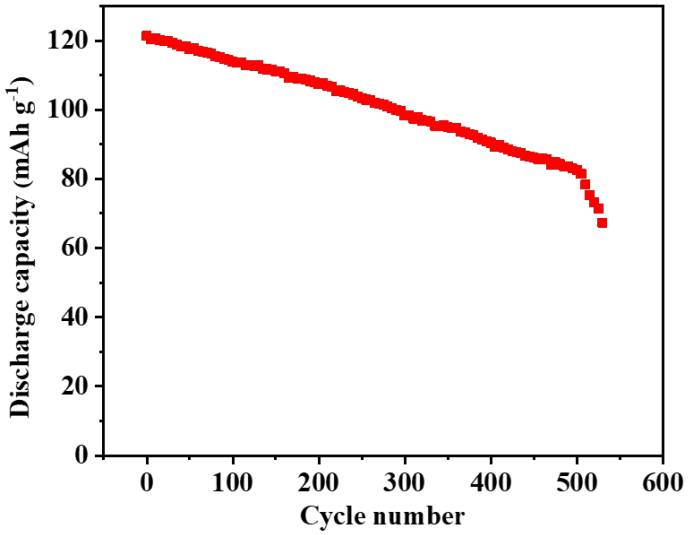

Figure S22. Cycling performance of LMO|AGM|Zn cell, employing CH as electrolyte additives under the same constrained condition in Figure 6a.

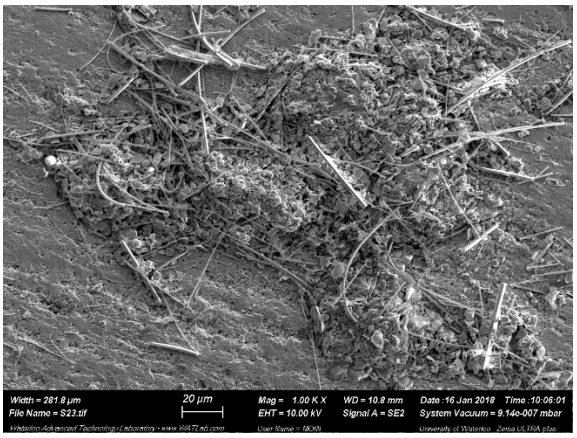

Figure S23. SEM image of Zn anode at 500th cycle in LMO|AGM|Zn cell, employing CH as electrolyte additives.

Figure S24. 80 cm^2 cathode sheet used in 5, 65 and 200 Ah industrial-level LMO|AGM+CH@AGM|Zn cells. Photo credit: Shengkai Li, University of Waterloo.

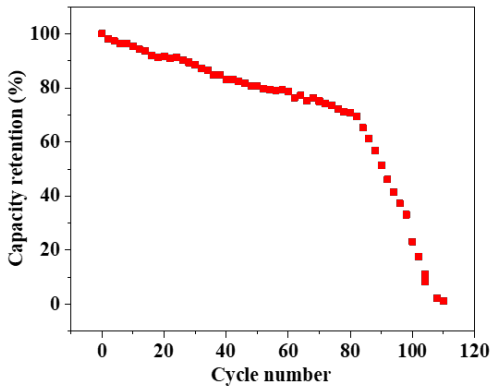

Figure S25. Cycling performance of the single battery unit from 200 Ah cell with strictly constrained electrolyte (3 g Ah^{-1}).

Table S1. Surface element atomic percentage of Zn metal anode in LMO|AGM+CH@AGM|Zn battery after different time chronoamperometry under 1M $ZnSO_4$ and 2M Li_2SO_4 electrolyte obtained from XPS spectra

Element	Atomic %	
	Zn anode after 5 minutes chronoamperometry	Zn anode after 10 minutes chronoamperometry
Zn	38.4	36.3
S	16.2	18.8
Li	11.4	7.1
N	-	3.2
O	16.8	14.3
C	17.2	20.3

Table S2. Surface element atomic percentage of Li metal anode in LMO|AGM+CH@AGM|Li battery after different time chronoamperometry under 1M $LiPF_6$ in 1:1:1 DMC:EC:DEC electrolyte obtained from XPS spectra

Element	Atomic %	
	Li anode after 20 minutes chronoamperometry	Li anode after 30 minutes chronoamperometry
Li	40.2	38.1
P	10.3	13.2
F	14.4	11.6
N	-	2.8
O	15.3	16.1
C	19.8	18.5

Table S3 Comparison of the thermodynamic parameters, obtained by ITC, of different cation-ligand interactions[a]

	n	K(M^{-1})	ΔH(kcal mol^{-1})
$ZnSO_4$→Gly-Pro-Ala	0.87±0.07	$1.13\times10^6\pm 0.12\times10^6$	-5.63±0.02
Li_2SO_4→Gly-Pro-Ala	0.93±0.04	$4.38\times10^6\pm 0.09\times10^6$	-2.21±0.05
$ZnSO_4$→colloidal SiO_2	1.12±0.02	$5.87\times10^4\pm 0.15\times104$	-1.28±0.06
Li_2SO_4→colloidal SiO_2	1.07±0.08	$3.22\times10^4\pm 0.21\times104$	-0.83±0.03

[a] Ligand and receptor solutions were prepared with the same buffer stock solution, 20 mM tris(hydroxymethyl)aminomethane (Tris) at pH 7.4.

Table S4. Cell parameters for various Zn metal batteries

	LMO|AGM+CH@AGM|Zn cell under unconstrained conditions[a]	LMO| AGM+CH@AGM|Zn cell under constrained conditions[a]	LMO| AGM+CH@AGM|Zn stacked cell (5Ah)[b]
Cathode capacity (mAh cm^{-2})	3.6	24	13.2[c]
Anode capacity (mAh cm^{-2})	147	58	147
Voltage (V)	1.8V	1.8V	1.8V
Total capacity (Ah)	0.014	0.216	5.28
Total cathode mass (g)	0.12	1.8	44
Total electrolyte mass (g)	0.42	2.16	79.2
Total anode mass (g)	1.6	0.642	76

Separator mass (g)	0.05	0.05	1.2
Brass mass (g)	0.03	0.03	1.6
Mass of package foil/tapes	0.02	0.02	0.5
Total weight (g)	2.24	4.702	203
Energy density (Wh kg^{-1})	11.25	80	46

[a] See Figure S6 for battery assembling configurations

[b] See Figure 6g

[c] See Figure S12 for cathode sheet

Table S5. Cell parameters for various Li metal batteries

	LMO| AGM+CH@AGM|Li cell under unconstrained conditions[a]	LMO| AGM+CH@AGM|Li cell under constrained conditions[b]
Cathode capacity (mAh cm^{-2})	1.8	24.6
Anode capacity (mAh cm^{-2})	51.5	51.5
Voltage (V)	4.1V	4.1V
Total capacity (Ah)	0.00171	0.0984
Total cathode mass (g)	0.014	0.8
Total electrolyte mass (g)	0.09	0.984
Total anode mass (g)	0.012	0.053
Separator mass (g)	0.01	0.03
Brass mass (g)	-	0.02
Mass of package foil/tapes	0.012	0.015
Total weight (g)	0.478	1.9
Energy density (Wh kg^{-1})	14	212

[a] CR2032 coin cell

[b] See Figure S6 for battery assembling configurations